ORNL/TM-2022/2683

Oak Ridge National Laboratory Multi material/functionally graded wire arc additive manufacturing of high strength steel valves clad with nickel alloy 625 used for oil extraction

CRADA Final Report NFE-20-08261

Andrzej Nycz
Clint Wildash
Yamamoto Yukinori
Luke Meyer
Derek Vaughan
Andres Marquez Rossy
Donovan Leonard

September 2022

OAK RIDGE National Laboratory

ORNL IS MANAGED BY UT-BATTELLE LLC FOR THE US DEPARTMENT OF ENERGY

ORNL/TM-2022/2683

Manufacturing Systems Research Division

MULTI MATERIAL/FUNCTIONALLY GRADED WIRE ARC ADDITIVE MANUFACTURING OF HIGH STRENGTH STEEL VALVES CLAD WITH NICKEL ALLOY 625 USED FOR OIL EXTRACTION

Author(s)

Andrzej Nycz
Clint Wildash
Yamamoto Yukinori
Luke Meyer
Derek Vaughan
Andres Marquez Rossy
Donovan Leonard

September 2022

Prepared by
OAK RIDGE NATIONAL LABORATORY
Oak Ridge, TN 37831

managed by
UT-BATTELLE LLC
for the
US DEPARTMENT OF ENERGY
under contract DE-AC05-00OR22725

CONTENTS

Contents

FIGURE CAPTIONS

TABLE CAPTIONS

ACKNOWLEDGEMENTS

This CRADA NFE-20-08261 was conducted as a Technical Collaboration project within the Oak Ridge National Laboratory (ORNL) Manufacturing Demonstration Facility (MDF) sponsored by the US Department of Energy Advanced Manufacturing Office (CPS Agreement Number 24761). Opportunities for MDF technical collaborations are listed in the announcement "Manufacturing Demonstration Facility Technology Collaborations for US Manufacturers in Advanced Manufacturing and Materials Technologies" posted at:

http://web.ornl.gov/sci/manufacturing/docs/FBO-ORNL-MDF-2013-2.pdf

The goal of technical collaborations is to engage industry partners to participate in short-term, collaborative projects within the Manufacturing Demonstration Facility (MDF) to assess applicability and of new energy efficient manufacturing technologies. Research sponsored by the U.S. Department of Energy, Office of Energy Efficiency and Renewable Energy, Advanced Manufacturing Office, under contract DE-AC05-00OR22725 with UT-Battelle, LLC.

ABSTRACT

This Phase 1 technical collaboration project (ORNL/TM-2022/2683) began on August 1st, 2020 and concluded on July 31st, 2022. The collaboration partner Schlumberger is a large business enterprise assisting oil companies to extract oil from land and subsea cost competitively and safely. It is based in Houston, Texas USA. In this work as study of additive deposition of AWS EF100S-G and AWS ERNiCrMo-3 wires via wire-arc process was conducted.

1. INTRODUCTION

1.1 BACKGROUND

The focus of this work is on the manufacture of high strength steel valves of various sizes (100lb to 5 tons) that are clad with nickel alloy (Inconel) 625 on internal and external features. The cladding enables safe high-pressure retention of extracted corrosive fluid (oil) and improves features such as ring grooves for wear connections, which enhances service life to provide lower cost improved corrosion and wear resistant surfaces. The improvement sought is to reduce manufacturing costs through a single stage multi material/functionally graded WAAM process, which will build up base metal and clad simultaneously. This new approach, not previously performed for this application, will be a significant improvement over the traditional three-stage manufacturing process: 1) forge base metal, 2) machine surfaces, and 3) clad with traditional wire arc processes. The novelty is reducing a traditional three-stage manufacturing process to a single stage manufacturing process creating a more cost-effective and energy efficient manufacturing technique. The other new aspect of this project was using a wire fed directed energy deposition process with Inconel 625 in a multi material printing scenario. ORNL is considered to have expertise in this area to better enable technical and commercial success in this endeavor as opposed to Schlumberger developing on its own. This is because it is challenging to perform the WAAM process using more than one material and achieve required volumetric and mechanical property acceptance criteria. Therefore, this technical collaboration served as an ideal opportunity to leverage both organizations' expertise to improve the U.S.'s manufacturing capabilities and achieve these criteria.

1.2 OBJECTIVE

In this study, LA100 (high-strength low alloyed steel wire based on HY-80, a commercial product from Lincoln Electric) was selected as the main body to be coated by Ni-base alloy 625. The source wires of LA100 and Alloy 625 were AWS EF100S-G and AWS ERNiCrMo-3, respectively. Typical alloy compositions of the materials are summarized in Table 1.

Table 1: Typical alloy composition of the material to be printed in the present study.

Material	Typical composition, wt.%											
	Fe	Ni	Cr	Mo	Mn	Si	C	Cu	Nb (+Ta)	Al	Ti	Co
LA100*	Bal.	1.88-1.96	0.04-0.06	0.43-0.45	1.63-1.69	0.46-0.50	0.05-0.06	0.11-0.14	-	0.01 max.	0.03-0.04	-
625*	0.4	64	21.7	8.5	0.1	0.14	0.02	0.01	3.8	0.1	0.17	0.5 max.

* Reference: https://www.lincolnelectric.com/en/Products/Filler-Metals

PHASE 1 TASK ACHIEVEMENTS

Task 1. (Schlumberger/ORNL) Provide acceptance criteria for additively manufactured functionally graded/mix material Inconel 625 high strength valves

Schlumberger provided the limitation of material dilution (the Ni content inside LA100, and the Fe content inside Alloy 625) to avoid defect formation, and acceptable interface morphology between LA100 and Alloy 625.

Task 2. (ORNL) Test feasibility of additive deposition of Nickel alloy 625, on base steel, by producing test sample of at least 3 inches tall

Alloy 625 blocks with ~4" tall were printed with various print conditions, mainly focusing on the shielding gas and trim. Optimized combination of the shielding gas (80% Ar + 20% He) and trim (= 1.0) were found and used for the following Alloy 625 printing tasks.

Task 3. (ORNL) Test feasibility of building multi material test sample by producing a sample wall of at least 3 inches tall of Inconel 625 clad on to and secondary material.

Multiple walls consisted of LA100 and Alloy 625 were printed with various combination of the print conditions targeting to produce defect-free materials suitable for subjecting mechanical property evaluation including tensile and Charpy impact toughness tests. The optimization of the print conditions was completed by a trial wall with a 2-inch tall without defect formation. The results also proved that the optimized print condition would be technically feasible in printing the defect-free, multi-materials walls more than 3 inches tall.

Task 4. (ORNL /Schlumberger/) Perform limited volumetric NDE such as Ultrasonic sound scan for bond integrity. Also, microstructure characterization of produced samples for example: optical/scanning electron microscopes, hardness distribution measurement, or monotonic compression tests and limited dilution and mechanical tests such as bend test.

NDE of the first multi-materials wall was completed by Schlumberger, which identified a large number of defects near the bond interface between LA100 and Alloy 625, attributed to the elemental dilution to each other through non-optimized print conditions. The cross-sectional microstructure characterization of the walls printed by both non-optimized and optimized processes was completed. By using the optimized print conditions found in Task 3, the "defect-free" multi-materials block for various mechanical property evaluations were ready to be produced.

Task 5. (Schlumberger/ORNL) Perform analysis of obtained results.

All walls printed in the present study were microstructurally and compositionally evaluated to identify the mechanism of defect formation at the interface between LA100 and Alloy 625 as a function of various print conditions. The obtained results strongly supported procedures established to optimize the print conditions to achieve the defect-free multi-materials block production.

2. TECHNICAL PROGRESS

2.1 ALLOY 625 PRINT OPTIMIZATION

This section summarizes a comparison of Ni-based alloy 625 blocks printed with different print conditions (shielding gas and trim) conducted at ORNL. The other print conditions (e.g., travel rate, wire feed rate, weld mode, bead inter-spacing, etc.) were kept the same at this stage, and used for further optimization of the print condition later. Blocks of size 2.5" in width x 8" in length x 4" in height were printed with total 5 different conditions, and the smoothness of the top surface was visibly inspected. It was found that a combination of "Trimix gas with medium power (trim = 1.0)" resulted in the best surface quality, and "80% Ar + 20% He mixed gas" achieved an acceptable surface quality equivalent to Trimix gas.

Figure 1 compares the top surface of the printed blocks with 5 different print condition (4 different shielding gases combining 3 different trims). The surface with pure Ar shielding gas (a) resulted in many craters due possibly to insufficient wettability of the print beads during printing process, which would cause the formation of internal voids beneath the next print layer. A mixed gas of 98% Argon + 2% CO_2 as a shielding gas (b and c) led to relatively continuous bead formation with lower amount of crater formation compared to pure Ar, although the surface quality was not sufficiently high to expect a defect (void)-free block production. The 98% Argon + 2% CO_2 mixed gas combined with 1.1 trim (high power) improved the surface quality with formation of very few craters (d). Trimix gas (90% He + 7.5% Ar + 2.5% CO_2) resulted in very smooth top surface, which would lead to very little chance of internal defect formation in the printed block. Table 2 summarizes the applied print conditions.

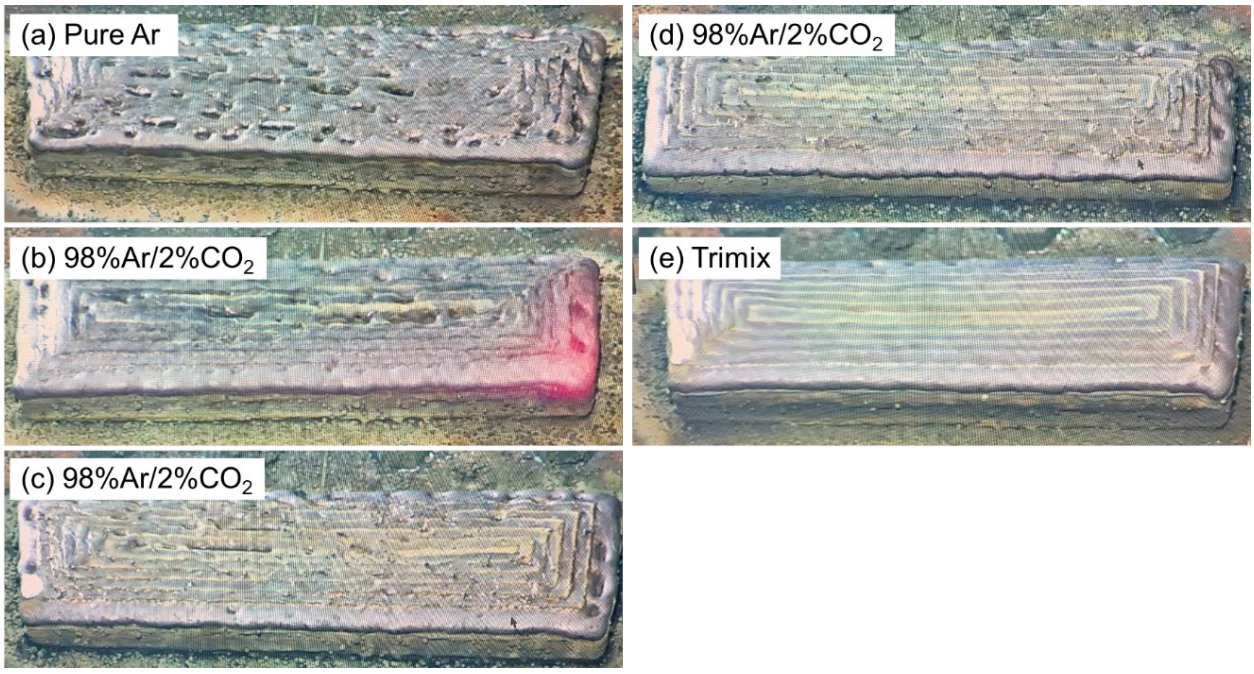

Figure 1: Alloy 625 printed blocks with various shielding gases and trims: (a) pure Argon gas with low power (trim = 0.9), (b) 98% Argon/2% CO_2 mix gas with low power (trim = 0.9, used a shop Ar gas), (c) 98% Argon/2% CO_2 mix gas with low power (trim = 0.9, used reserve Ar gas), (d) 98% Argon/2% CO_2 mix gas with high power (trim = 1.1), (e) Trimix gas with medium power (trim = 1.0).

Table 2: List of the print conditions used for Alloy 625 blocks

Block	Shielding gas	Trim	Weld mode	Travel speed (inch/min)	Wire feed (in/min)	Remarks
#1	Pure Ar	1.1 (high power)	503	40	400	Visible craters throughout, worst results
#2	98% Ar/2% CO_2 (Shop Ar)	0.9 (low power)	503	40	400	Large visible craters in the center and edges
#3	98% Ar/2% CO_2 (Reserve Ar)	0.9 (low power)	503	40	400	Less craters in the center, still not dense
#4	98% Ar/2% CO_2 (Reserve Ar)	1.1 (high power)	503	40	400	The best result with Ar/CO2
#5	Trimix	1.0 (Medium power)	503	40	400	Consistent results with a dense part

The results above suggested that the He-containing shielding gas could be beneficial for obtaining high surface quality with less chance of internal defect formation. However, helium gas is expensive and will raise the production cost. Therefore, additional study was conducted to identify a low He-containing gas with a print quality comparable to that of Trimix gas. Figure 2 shows Alloy 625 blocks printed with shielding gases with various He contents. Note that they were printed with the identical print conditions of the block #5 in Table 2, except for the shielding gas. In comparison with block #5 (a), 90%He, block #6 with a 96% Ar +4% He mixed gas (b) resulted in a non-smooth bead surface with formation of a few voids on the top surface. The block #7 with 80% Ar + 20% He mixed gas (c), on the other hand, showed a smooth top surface equivalent to Trimix. The cross-sectional macroscopic characterization (not shown) indicated that block #6 with 4% He showed some voids internally. On the other hand, block #7 with 20% He showed no visible void, which was same as the void-free cross-section of block #5 with 90% He. Based on these results, “80% Ar + 20% He mixed gas” combining with “trim 1.0” were chosen for the base-line print condition for Alloy 625 in the present study.

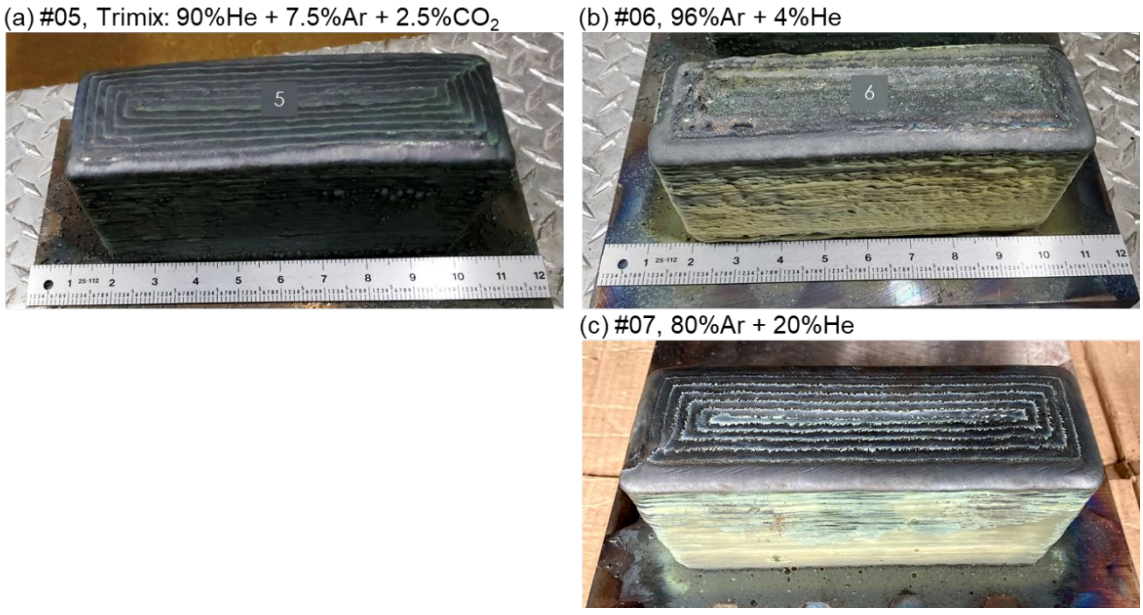

Figure 2: Alloy 625 blocks with various shielding gas: (a) Trimix, (b) 96% Ar + 4% He, and (c) 80% Ar + 20% He.

2.2 MULTI-MATERIALS PRINT WITH CONVENTIONAL (NON-OPTIMIZED) PROTOCOL

This section summarizes the characterization results of the multi-material print (LA100 and Alloy 625) with a conventional (non-optimized) print procedure. Two wall products consisting of Alloy 625 on LA100 with a horizontal interface were successfully fabricated without formation of any critical defects (e.g., cracks) on or adjacent to the interface, possibly due to a very limited Ni dilution inside LA100. On the other hand, a block product with an alternative print of LA100 and Alloy 625 side-by-side resulted in the formation of many cracks inside LA100 at the interface. It was due to a significant amount of the Ni dilution inside LA100, and an inter-spacing of 4.5 mm between both materials which might have been too close and promoted a mixture of LA100 and Alloy 625 at the interface. The hardness measurement and the compositional analysis near the interface supported the mechanism of the crack formation.

Figure 3 represents a picture of the printed multi-materials walls (A) and block (B) consisting of LA100 and Alloy 625 (a), together with cross-sections of the wall A (b) and the block B (c) sectioned ~2-inch away from the edge. The latter was printed with 4.5 mm bead-to-bead spacing, including the spacing between LA100 and Alloy 625. The other print conditions are summarized in Table 3. Metallographic specimens to observe the detailed microstructure across the interface were removed from the red rectangle areas in the images.

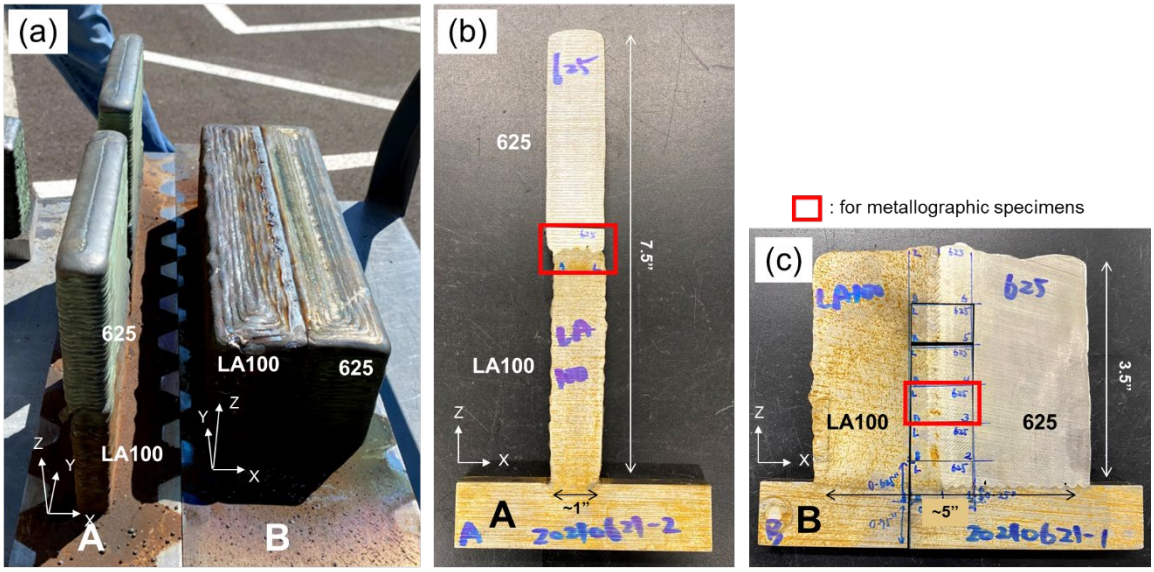

Figure 3: A picture showing the printed multi-materials walls and block with Alloy 625 and LA100 (a), and cross-sections of the wall (b, called as "A") and the block (c, called as "B"). The rectangles with red line in b and c represent the locations of the metallographic specimens shown in Figure 5.

Table 3: List of the print conditions used for the multi-materials wall (A) and block (B)

Wall	Wire	Inter-spacing between 625 and LA100	Shielding gas	Trim	Weld mode	Travel speed (inch/min)	Wire feed (in/min)	Remarks
A	LA100	N.A.	98% Ar/2% CO_2	1	18 (Rapid arc)	40	400	4.5mm bead-to-bead spacing and ~2mm layer height
	625		80% Ar/20% He	1	503 (Pulse)	40	400	
B	LA100	4.5 mm	98% Ar/2% CO_2	1	18 (Rapid arc)	40	400	
	625		80% Ar/20% He	1	503 (Pulse)	40	400	

After sectioning the metallographic specimens at ORNL, the wall A and the block B were delivered to Schlumberger for non-destructive evaluation. The surfaces were machined to make them flat and clean, and then a dye penetration inspection was applied, as shown in Figure 4. The wall A (a) showed only two isolated defects at the interface between LA100 and Alloy 625, which corresponded to bubbles formed on the interface or incomplete fusion of Alloy 625 beads onto LA100. Note that they were considered to be easily eliminated by fine-tuning the print conditions (e.g., controlling inter-pass temperature). On the other hand, the block B (b) exhibited two aligned defects parallel to, but with a slight offset from, the interface. The defects were also observed in the other side of the machined block, suggesting that they exist in the whole length of the block. Because of the defects, the planed property evaluation (compression/tensile tests and Charpy impact toughness tests at room temperature) was cancelled, and the major target was shifted to characterize the details of the defects and identify the source of the defect formation.

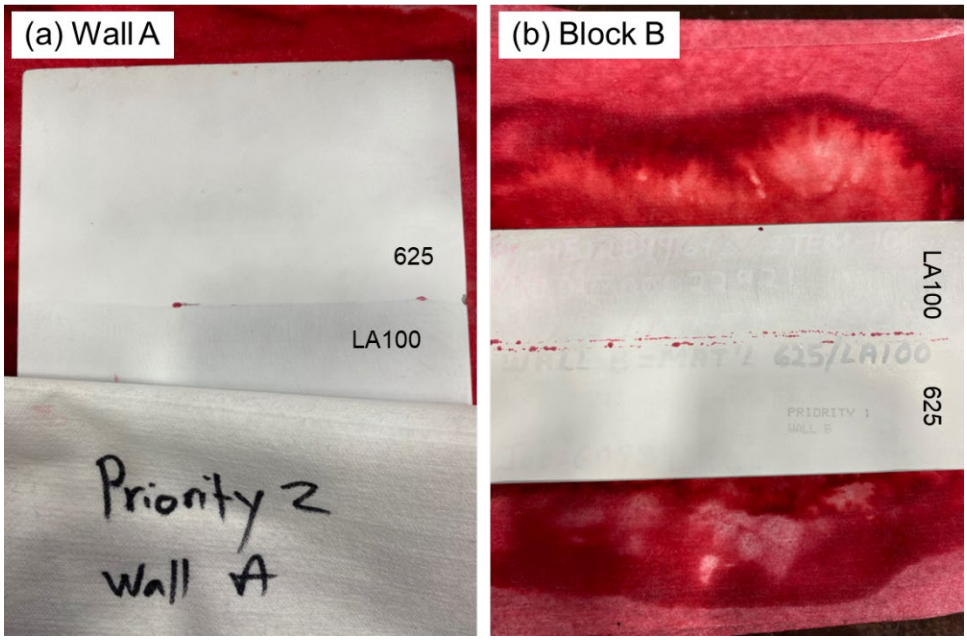

Figure 4: The dye penetration inspected multi-materials printed products: (a) the wall A, and (b) the block B (the inspection was conducted by Schlumberger).

The close observations near the interface are shown in Figure 5. The wall A showed a distinct interface between LA100 and 625 with no cracks near the interface. A pore was observed on the interface, although such voids were considered to be easily eliminated by tweaking the print condition. The block B, on the other hand, showed no clear interface between LA100 and Alloy 625 but was discontinuous with gradual contrast changes, especially in the LA100 side, near the interface. Each print bead was visible in the LA100 after etching with 5%Nithal, representing mostly a ferritic-martensitic microstructure or mixed with untransformed austenite grains. Many cracks were accumulated in the LA100 beads adjacent to the interface (Bead 2 in “b”).

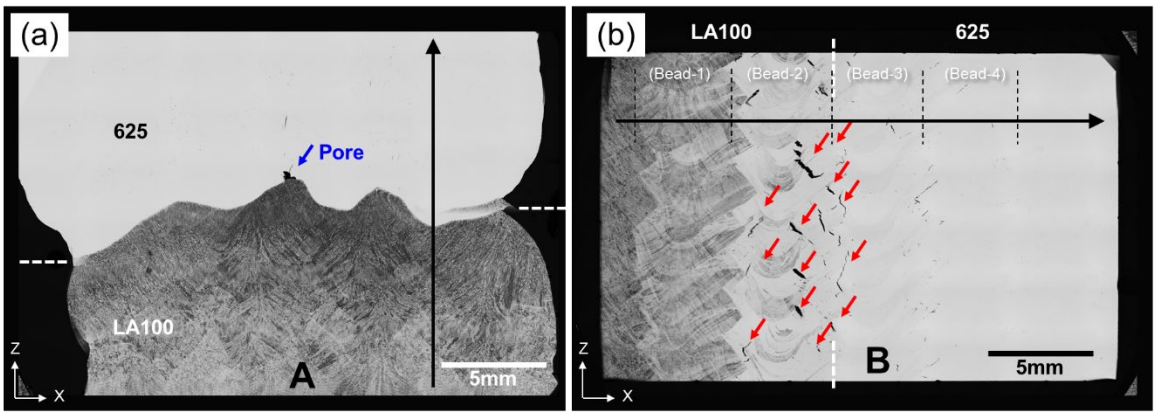

Figure 5: Cross-sectional micrographs near Alloy 625-LA100 interface in (a) the wall A and (b) the block B. The blue and red arrows indicate a pore and cracks observed in the cross-sections. The black arrows correspond to the lines conducted micro-Vickers hardness measurements and chemical analysis by SEM-EDS.

The micro-Vickers hardness and the Ni- and Fe-contents measured by SEM-BSE along the black arrows in the cross-sections are shown in Figure 6. In the wall A, the hardness was mostly unchanged in the LA100 side, and a slight hardness drop was observed just above the interface. This was due to dilution of Fe in LA100 that occurred in the Alloy 625 layer just above the interface, although the amount of Fe did not cause a significant microstructural change affecting the hardness. In the other words, the Ni-reduction in Alloy 625 down to ~30 wt.% (Note: nominal Ni content in Alloy 625 is ~60 wt.%) did not significantly impact con microstructure or the hardness.

On the other hand, the block B exhibited a significant increase in hardness in the LA100 side as well as hardness scattering in the adjacent bead in the Alloy 625 side. The composition analysis clearly revealed the Ni-dilution in LA100 and the Ni-reduction in Alloy 625 near the interface: less than 5 wt.% Ni-dilution in Bead 1 region, 5-15 wt.% Ni-dilution in Bead 2, and only 10-30 wt.% Ni-remnant in Bead 3. The hardness changes in LA100 indicated that the Ni-dilution in LA100 increased the hardenability by promoting martensitic transformation, and that 5-15 wt.% of the Ni content in LA100 could lead to the crack formation during printing process due to its excess hardness. It should be emphasized that a few cracks were also observed in Bead 3 region which correspond to Alloy 625 with a significant amount of Fe-dilution. Because of very low Ni content compared to nominal Ni contents in All 625, a part of Bead 3 regions also consisted of very hard martensitic microstructure (as considered from the hardness scattering in the region) and promoted a dispersion of cracks.

Based on these findings (as well as the provided criteria from Schlumberger), the print conditions and procedure needed to be optimized to avoid such elemental dilution inside LA100 (as well as inside of Alloy 625). Hereafter, the optimization study focused on the inter-spacing between LA100 and Alloy 625, alternative print procedure, inter-pass temperatures, weld mode, and so on, to minimize or eliminate the elemental dilutions in both materials.

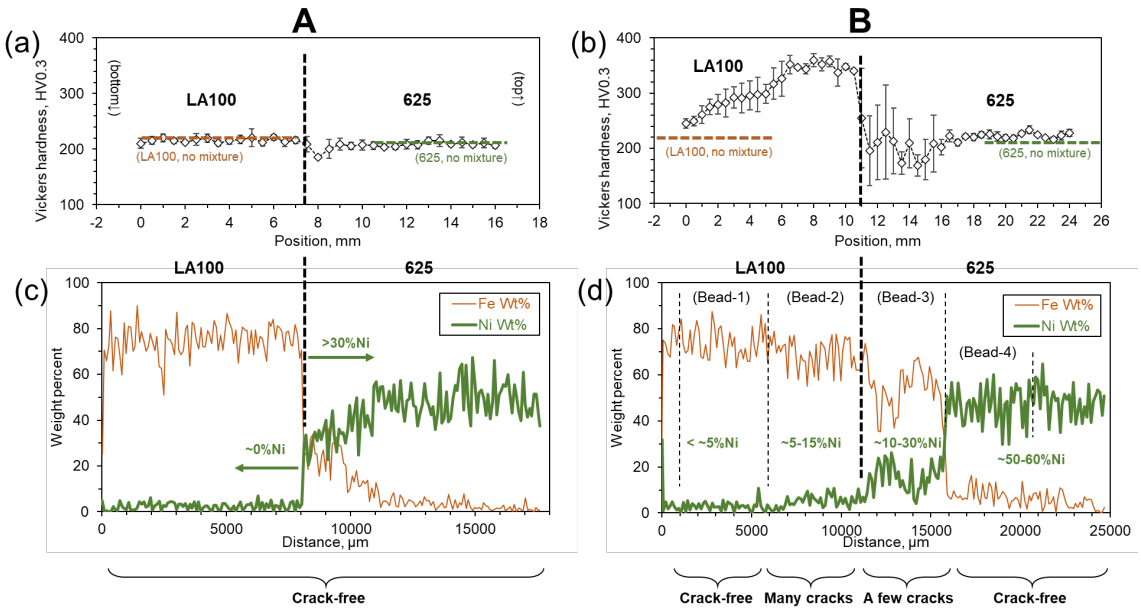

Figure 6: Micro-Vickers hardness (a, b) and Ni- and Fe-composition profiles (c, d) along the lines shown in Figure 6: (a, c) the wall A, and (b, d) the block B.

2.3 EFFECT OF VARIABLES ON ALLOY 625-LA100 INTERFACE

This section summarizes microstructural responses in multi-materials print with various print conditions, in order to find an optimized print procedure to achieve a good adhesion of both materials together with minimized elemental dilution to avoid any defect formation inside the print beads. The print conditions of interest include the inter-spacing between LA100 and Alloy 625, an alternative print procedure, inter-pass temperatures, weld mode, and so on. All printed walls were built after multiple single bead trial prints with small variations of the print conditions (trim, travel speed, wire feed rate, weld mode, inter-pass temperatures), and then the best condition was chosen for printing the multi-materials wall. After a visible inspection of the wall interface whether the interface was physically contacted or not, cross-sectional microstructure observations by optical or scanning electron microscopes were conducted for further evaluation. The print conditions evaluated in the present study are summarized in Table 4.

Table 4: List of the print conditions used in the present study

Wall	Wire	Inter-spacing between 625 and LA100	Shielding gas	Trim	Weld mode	Travel speed (inch/min)	Wire feed (in/min)	Remarks
#1	LA100	5mm, 5.5mm, and 6mm	98% Ar/2% CO_2	1	18 (Rapid arc)	40	400	ORNL trial wall 2
	625		80% Ar/20% He	1	503 (Pulse)	40	400	
#2	LA100	5mm	98% Ar/2% CO_2	1.1	309 (STT)	20	225	ORNL trial wall 3, #4 (#20211102), 200°C inter-pass, 30-degree inclined
	625		80% Ar/20% He	1	75 (CV)	40	200	
#3	LA100	5mm	98% Ar/2% CO_2	1.1	309 (STT)	20	225	ORNL trial wall 3, #5 (#20211102), 200°C inter-pass
	625		80% Ar/20% He	1	503 (Pulse)	40	400	
#4	LA100	5mm	98% Ar/2% CO_2	1.1	309 (STT)	20	225	

	625		80% Ar/20% He	1	75 (CV)	40	200	ORNL trial wall 3, #3 (#20211102), 200°C inter-pass
#5	LA100	5mm	98% Ar/2% CO_2	1	309 (STT)	20	225	ORNL trial wall 5, 5mm (#20220203)
	625		80% Ar/20% He	1	75 (CV)	40	200	
#6	LA100	5.5mm	98% Ar/2% CO_2	1	309 (STT)	20	225	ORNL trial wall 5, 5.5mm (#20220203)
	625		80% Ar/20% He	1	75 (CV)	40	200	
#7	LA100	6mm	98% Ar/2% CO_2	1	309 (STT)	20	225	ORNL trial wall 5, 6mm (#20220203)
	625		80% Ar/20% He	1	75 (CV)	40	200	

2.3.1 Offset and inter-spacing between Alloy 625 and LA100

The elemental dilution would occur when the print beads physically contacted with the other material and melted it during printing process. To avoid such situation, especially for Ni-dilution in LA100, multiple-layers offset during the alternative print process of LA100 and Alloy 625 was proposed, in which the Alloy 625 layer would be printed while maintaining 2 layers behind the LA100 layer, as illustrated in Figure 7. The proposed process would eliminate or minimize the potential physical contact of the LA100 print bead to the Alloy 625 substrate, and therefore the Ni-dilution as well. Although the Alloy 625 print bead will physically contact the LA100 substrate during printing process, the lower melting point of Alloy 625 than LA100 (~1300 and ~1600°C, respectively) should allow brazing Alloy 625 adjacent to the printed LA100 without melting LA100, and therefore eliminating or minimizing the Fe-dilution in Alloy 625. It should be noted that the offset with more than 2 layers would interfere with the print process because of a physical contact of the weld torch gas nozzle with the printed LA100. Therefore, the trial wall was made with an offset of 2-layers.

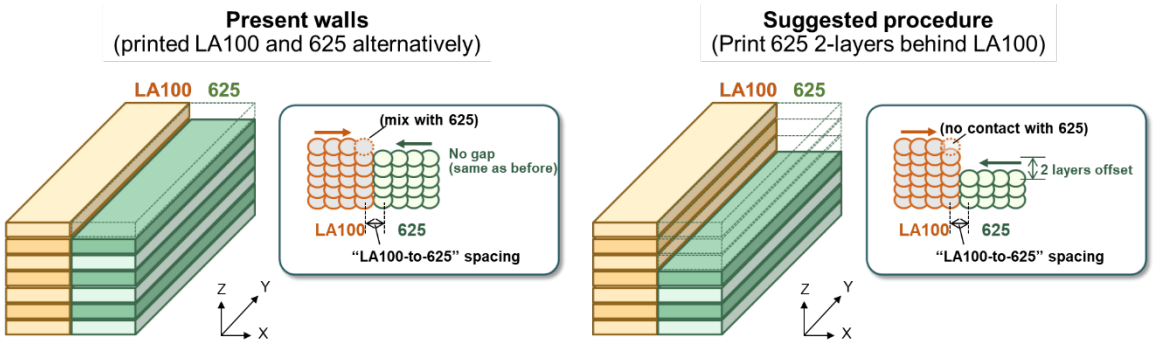

Figure 7: Illustration explaining normal alternative print process and 2-layers offset print process.

The trial wall #1 with the 2 layers of offset in Alloy 625, together with three different inter-spacings between LA100 and Alloy 625, was printed as shown in Figure 8. Each region with a constant inter-spacing has a 3-inch length, and three different regions were continuously printed, so that the other print conditions other than the inter-spacing were considered mostly identical to each other (e.g., thermal history, etc.). The optical micrograph of the cross-section at each inter-spacing, shown in (b), exhibited a microstructurally redundant region at around 0.5-inch from the bottom, in which the printed materials were rapidly cooled by the fast heat escape through the base plate. The region showed open voids (highlighted by red) along the interface as an incomplete adhesion of LA100 and Alloy 625, possibly caused by the rapid cooling. Above the redundant region, the heat-flow is considered stable, which allows to discuss the effect of the inter-spacings on the microstructure.

The cross-sectioned images showed obvious differences in the microstructure with the inter-spacings. In 5mm spacing, the LA100 bead adjacent to the interface showed a significant Ni-dilution together with some cracks inside the beads, suggesting that 5mm inter-spacing was not sufficiently wide to avoid the mixing with Alloy 625, even with applying 2-layers' offset. In 5.5mm spacing, the Ni-dilution was still observed in LA100, although contrast of the mixed region was slightly weaker than the 5mm spacing, suggesting that the amount of the Ni-dilution was qualitatively lower than that with the 5mm spacing. It should be emphasized that some of the voids were observed at the interface. In 6mm spacing, the Ni-dilution in LA100 became relatively low compared to that with the 5.5mm spacing, although the incomplete adhesion at the interface was also observed as elongated open voids.

Each bead has around 2mm height during the present printing process, so that the 2 layers of offset would give ~4mm height gap between LA100 and Alloy 625. In the present results, the gap seems insufficient to avoid a physical contact of the print bead of LA100 with Alloy 625. The Ni-dilution reduced with increasing the inter-spacing from 5mm to 6mm, although the larger inter-spacing also promoted the formation of incomplete adhesion of the interface between LA100 and Alloy 625. Since the redundant region also showed the incomplete adhesion at the interface, the controlled inter-pass temperature could also be an important factor.

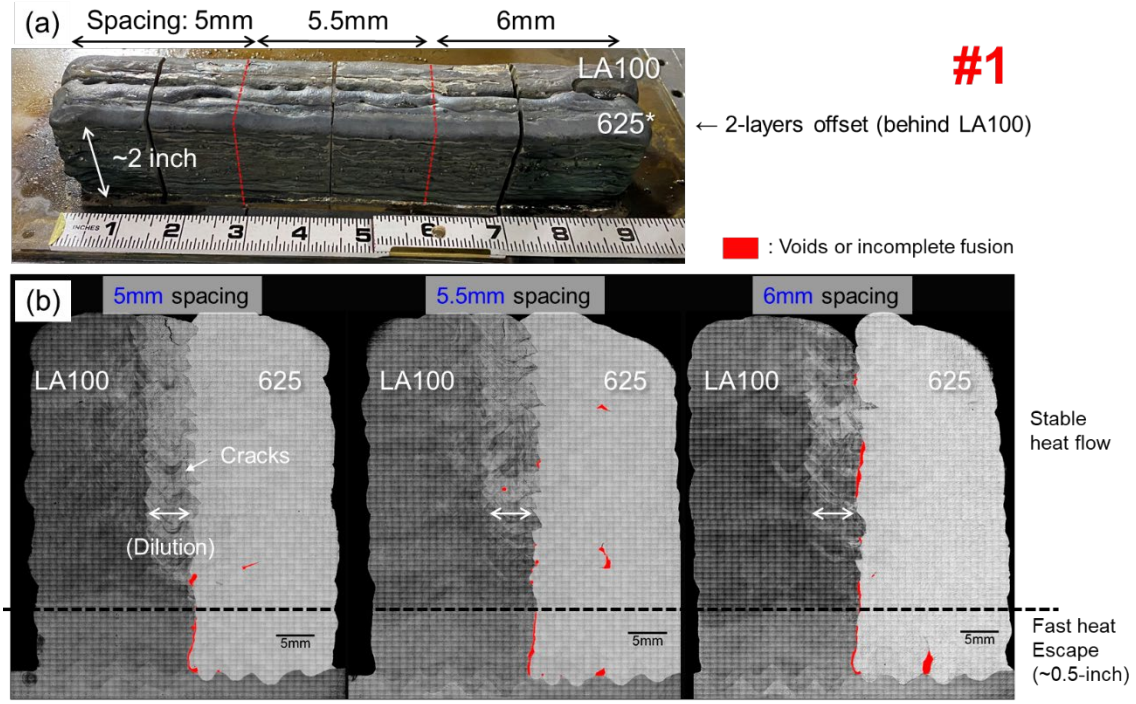

Figure 8: (a) A picture showing the trial wall #1 which applied 2-layers offset of Alloy 625 together with three different inter-spacing, and (b) cross-sectional micrographs at each center of the printed wall.

To increase the height gap, an inclined torch was also attempted to allow more offset between LA100 and Alloy 625. Figure 9 illustrates the configurations of the trial wall #2 with 4-layers offset by applying 30-degree torch angle, together with the actual printed wall with 5mm inter-spacing and the cross-sections of the wall. The interface adhesion was incomplete and unstable since the control of the distance between the inclined torch and the substrate was technically difficult. Based on these results, multi-layers offset approach is considered not feasible to control the interface adhesion between LA100 and Alloy 625.

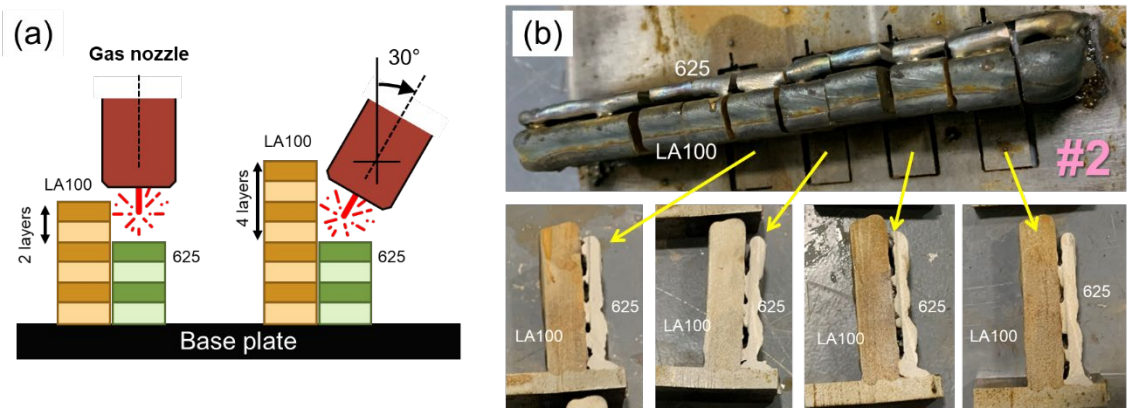

Figure 9: (a) the print configuration of the trial wall #2 with 4-layers offset combining with 30-degree inclined torch, and (b) pictures showing the wall and cross-sections.

2.3.2 Weld mode (for Alloy 625)

The trial walls #3 and #4 investigated the effect of the weld mode for Alloy 625, a pulse mode and a CV mode, respectively, on the quality of the interface adhesion. The other conditions were kept constant, such as no layer offset, no torch angle, 5mm inter-spacing, and a constant inter-pass temperature at 200°C (note: the 200°C inter-pass temperature was selected as "cold" print targeting to reduce the wettability of Alloy 625 print beads). Alloy 625 in the trial walls #1 and #2 was also printed with the pulse mode, so that the trial wall #3 would also demonstrate the effect of the controlled inter-pass temperature, instead of the multi-layers offset, on the interface quality.

Figure 10 compares the printed walls and the cross-sections between the trial walls #3 (a) and #4 (b). The trial wall #3 showed almost no obvious Ni-dilution in LA100 (except for a few beads with a dark contrast, as well as the cross-section near the wall edge). The change in the weld mode from the pulse mode to the CV mode in the trial wall #4 did not show a significant change in the macroscopic characteristics of the cross-sections. The magnified images of the cross-sections near the center of the wall lengths are shown in Figure 11. By enhancing the image brightness, the trial wall #3 revealed significantly large amount of incomplete adhesion at the interface, whereas the amount of such region was very limited in the trial wall #4. The Ni dilution in LA100 seems very similar to each other, suggesting that the CV mode would be more optimal than the pulse mode for the improved adhesion while maintaining a limited Ni-dilution.

The compositional analysis by SEM-EDS was conducted, as summarized in Figure 12. The 2D compositional distribution of Fe and Ni qualitatively revealed that the Ni-dilution in LA100 (as well as the Fe-dilution in Alloy 625) were very limited, especially in the area highlighted by the yellow circle, as opposed to the macroscopic observation in Figure 10. The quantitative analysis by line analysis demonstrated that the Ni-dilution in LA100 is not obvious and the amount of Ni is equivalent to that far from the interface. The detailed microstructure observation also revealed that there was no crack inside the beads, suggesting that the correlation with the limited Ni-dilution and crack-free beads are consistent with the discussion in Figure 5.

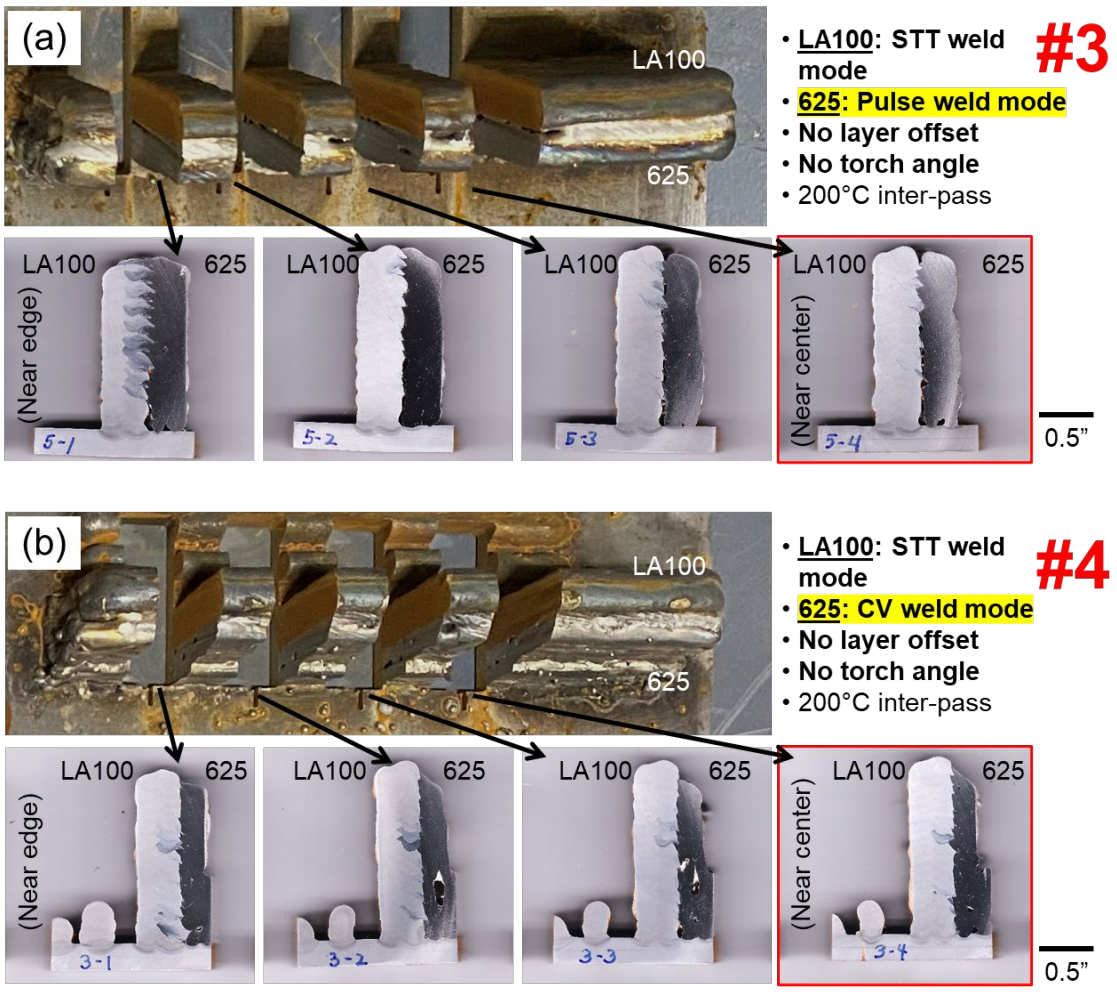

Figure 10: Pictures showing the trial walls and their cross-sections: (a) trial wall #3, and (b) trial wall #4.

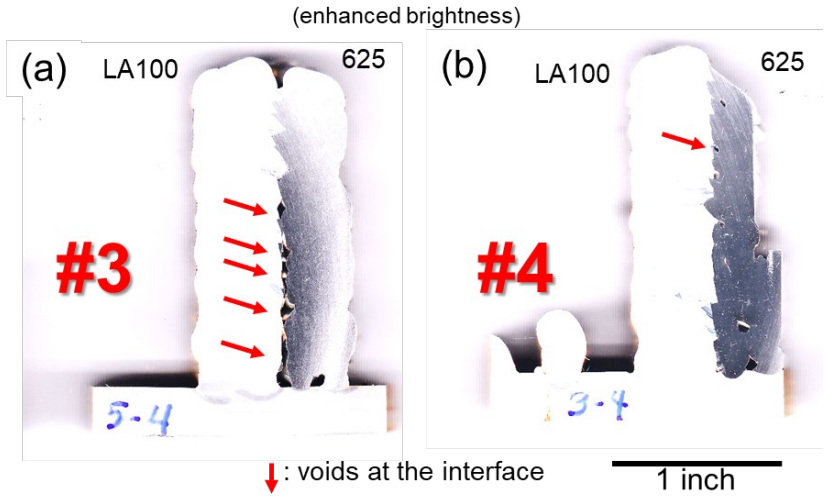

Figure 11: Cross-sections of the trial walls near center of the wall lengths: (a) trial wall #3, and (b) trial wall #4.

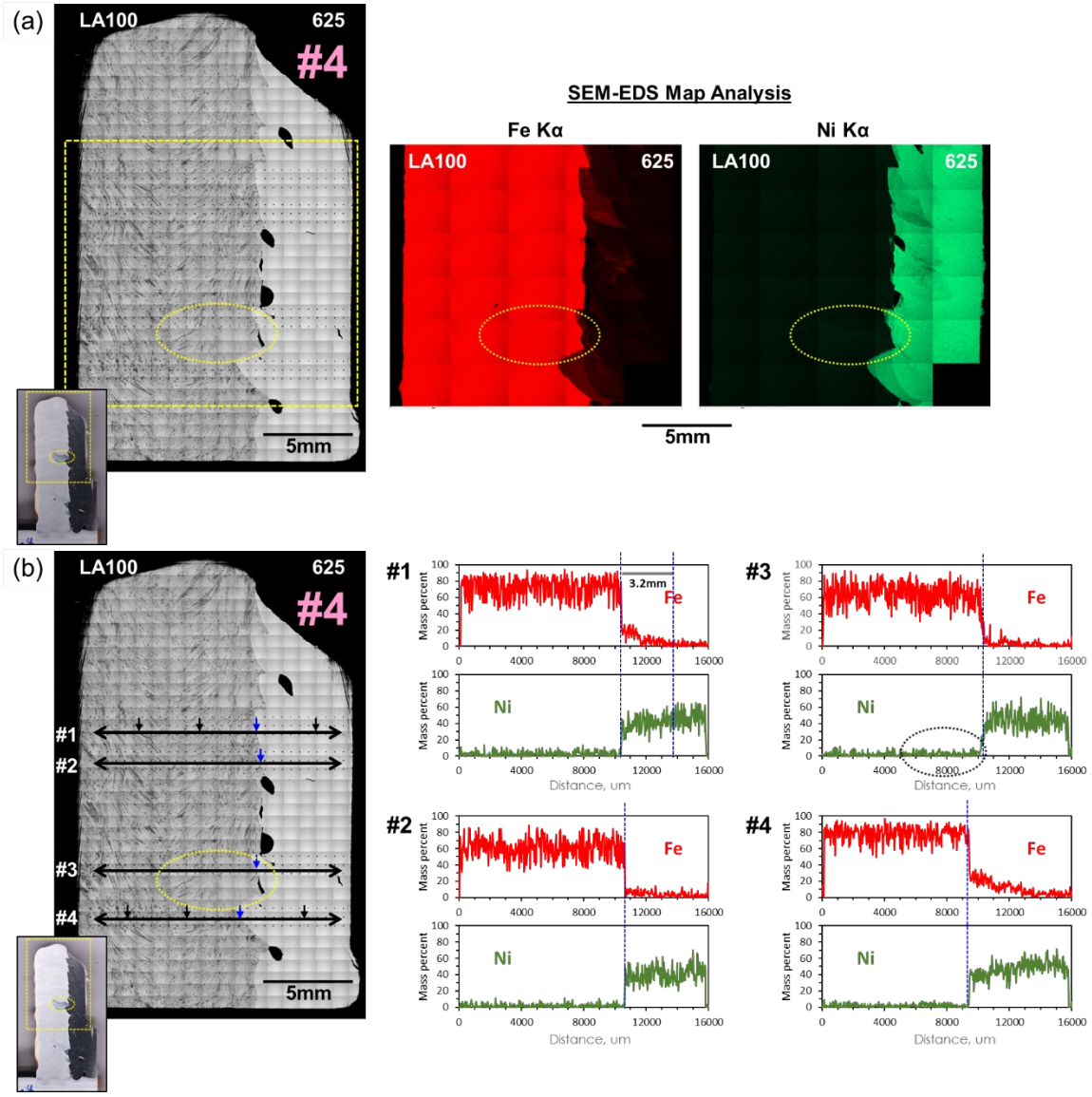

Figure 12: (a) SEM-EDS map analysis results showing 2D compositional distribution of Fe and Ni in the trial wall #4, and (b) SEM-EDS line analysis results showing Fe- and Ni-compositional profile along the lines #1 through #4 in the trial wall #4.

2.3.3 Spacing calibration

All the obtained results including the combination of the print conditions with no layer offset, no torch angle, printing Alloy 625 with the CV mode, and keeping the inter-pass temperature at 200°C were found to lead to a better interface adhesion without a significant amount of the Ni-dilution in LA100. However, to eliminate the void formation at the interface between LA100 and Alloy 625, as observed in Figure 11 and Figure 12, would require further optimization of the print condition.

Since the optimized combination of the print conditions is proposed, the geometrical factor needs to be re-visited as one of the important print conditions. The multi-material print of LA100 and Alloy 625 with

various inter-spacing was conducted with the optimized print conditions found in the previous section. Figure 13 summarizes the detailed print conditions with four different inter-spacings, 5mm, 5.5mm, 6mm, and 7mm. Note that the 7mm inter-spacing was found too wide to expect a physical contact of the two different materials, such that no wall was printed with that inter-spacing. The trial walls with the other three inter-spacings were printed with 8-inch length and 2-inch height, and the cross-sectional microstructure characterization was conducted near the center of the wall length.

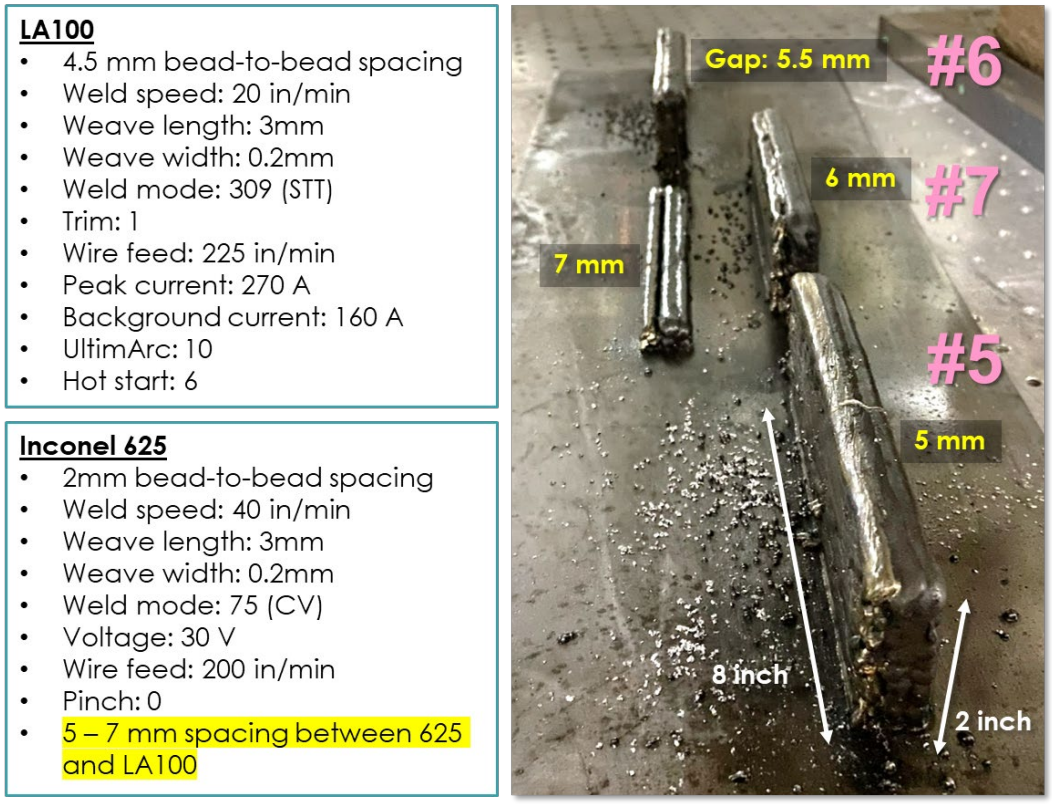

Figure 13: Re-optimization of the inter-spacing between LA100 and Alloy 625 with the optimized print conditions.

Figure 14 compares the etched cross-sections prepared from the as-printed trial walls. The trial wall #5 with 5mm spacing showed the Ni-dilution in LA100, although no cracks were observed in the cross-section. The trial wall #6 with 5.5mm spacing also showed the Ni-dilution, although the amount of the dilution reduced compared to the trial wall #5. A few small voids were observed near the interface, although they were not correlated with the incomplete adhesion but rather formed as bubbles inside the print beads and could be eliminated by further print optimization (e.g., slower deposition rate). The trial wall #6, on the other hand, exhibited almost no contrast change in the LA100 beads, suggesting very limited Ni-dilution in LA100.

A metallographic specimen was sectioned from the trial wall #6 for further detailed microstructure characterization. The as-polished cross-section, shown in Figure 15, indicated a distinct interface between LA100 and Alloy 625 with no contrast changes in both sides, no incomplete adhesion, and no crack formation near the interface. Two yellow lines in the image correspond to the locations where the SEM-EDS line analysis was conducted.

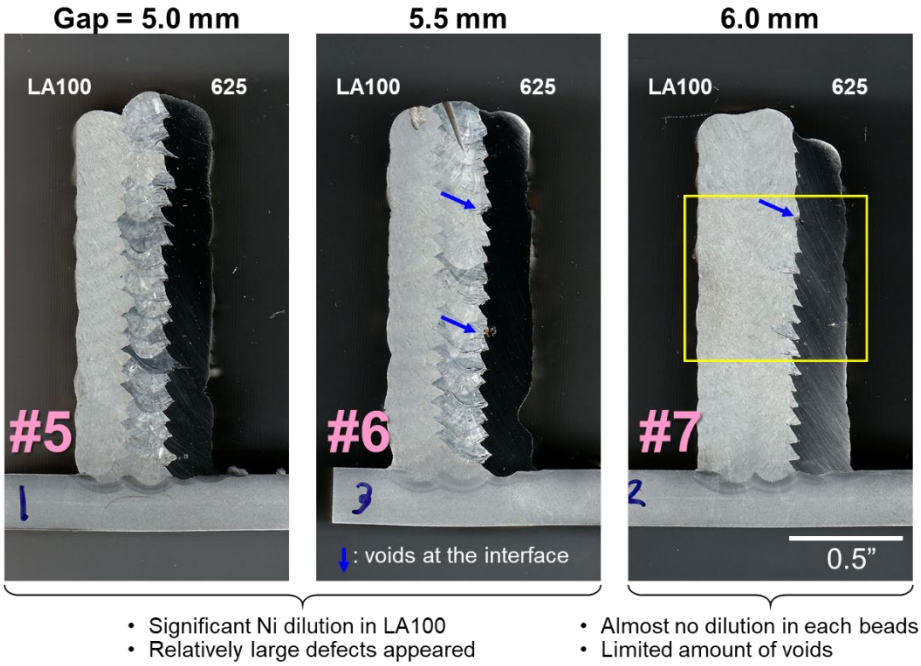

Figure 14: Cross-sections of the trial walls #5 through #7, sectioned from near center of the wall lengths.

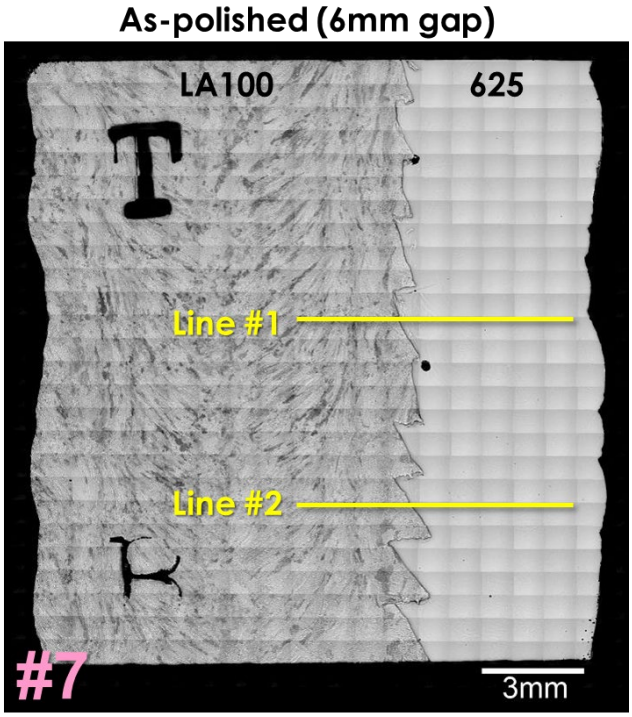

Figure 15: As-polished metallographic specimens of the trial wall #7. Two lines in the image correspond to the locations of SEM-EDS line analysis.

Figure 16 summarizes the compositional analysis across the interface between LA100 and Alloy 625. The map analysis near the line #1 (a) indicated a relatively wide distribution of Fe in Alloy 625. The line analysis suggested nearly 10% of Fe-dilution occurred in the Alloy 625 bead from the interface to ~4mm away from the interface, suggesting that the dilution occurred only in the first beads of Alloy 625 adjacent to the interface. A limited Ni-dilution was also observed in LA100, although the amount of Ni content was less than 5 wt.% near the interface and majority in LA100 did not show a sign of Ni-dilution. The analysis at the line #2 (b) was also identical to that in the line #1.

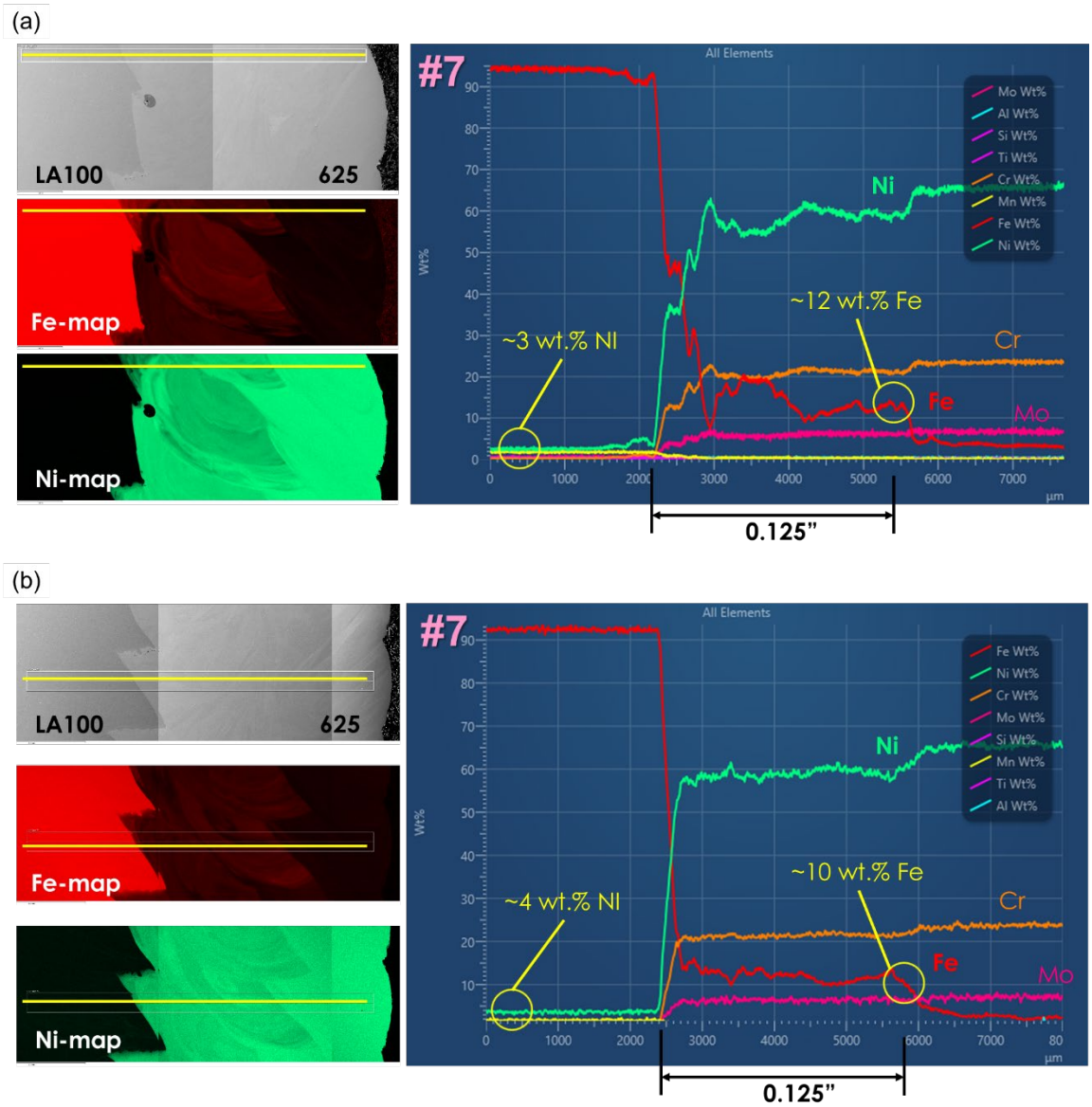

Figure 16: SEM-BSE/Fe-map/Ni-map/composition profiles: (a) along the line #1 and (b) along the ling #2, designated in Figure 15.

Schlumberger also performed compositional analysis in house by optical emission spectroscopy (OES). The specimen that was presented in Figure 15 and Figure 16 was used for the analysis at Schlumberger. Two locations inside Alloy 625 were selected for the analysis; one on the line at 1.25-inch (~32 mm) away from the peak height of LA100/Alloy 625 interface and the other on the line at the same distance

but from the lowest height of the interface as shown in Figure 17. The obtained compositions are summarized in Table 5, which indicates that the Fe and Ni contents are nearly 4 wt.% and 60 wt.%, respectively, for both locations. The measured Fe contents at both locations were lower than the results in Figure 16 by SEM-EDS but rather closer to the contents inside the second beads in Alloy 625. The measured Ni contents were consistent with the SEM-EDS results. These results suggest that the position at 1.25-inch away from the interface was considered as a transition line between the first and the second beads of Alloy 625 adjacent to LA100, although the Fe dilution (and the Ni reduction) could be between ~4-12% which would not become the source of defect formation, based on the characterization in the present study.

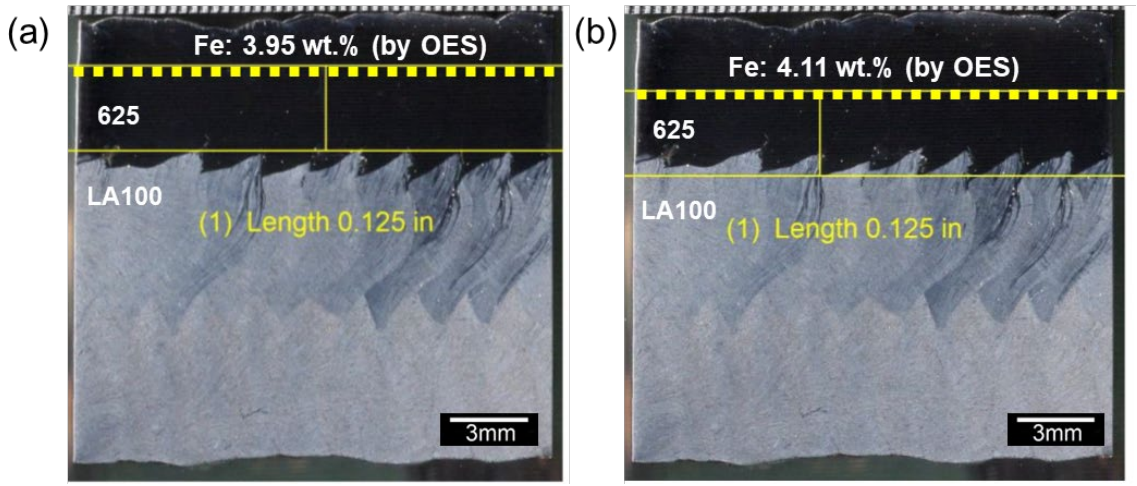

Figure 17: Locations conducted the OES compositional analysis (provided by Schlumberger).

Table 5: Analyzed compositions in two different locations in Alloy 625

Location	Analyzed composition, wt.%					
	Cr	Ni	Mo	Fe	Nb	C
Line (a)	22.18	60.39	8.24	3.95	3.19	0.019
Line (b)	22.91	59.71	8.67	4.11	3.16	0.018

In summary, the combination of the present print condition was optimal to avoid the crack formation attributed to the elemental dilution in both materials, and near 10 wt.% of Fe-dilution would be acceptable range for crack-free print of Alloy 625 onto LA100.

3. CONCLUSIONS

The purpose of this technical collaboration between ORNL and Schlumberger was to test the practical feasibility of using wire-arc technology to produce multi material structures. In this study process conditions for the nickel alloy 625 were optimized as well as multi-material with LA100. A detailed metallographic analysis and further optimization were performed and showing the feasibility of using the two materials for additive manufacturing.